

Electronic structure of superconducting KC_8 and non-superconducting LiC_6 graphite intercalation compounds: Evidence for a graphene-sheet-driven superconducting state

Z.-H. Pan,¹ J. Camacho,¹ M.H. Upton,² A. V. Fedorov,³ C.A. Howard,⁴ M. Ellerby,⁴ and T. Valla^{1,*}

¹*Condensed Matter Physics and Materials Science Department, Brookhaven National Lab, Upton, NY 11973*

²*Advanced Photon Source, Argonne National Laboratory, Argonne, IL 60419*

³*Advanced Light Source, Lawrence Berkeley National Laboratory, Berkeley, CA 94720*

⁴*London Centre for Nanotechnology and Department of Physics and Astronomy, University College London, London WC1E 6BT, United Kingdom*

(Dated: October 25, 2018)

We have performed photoemission studies of the electronic structure in LiC_6 and KC_8 , a non-superconducting and a superconducting graphite intercalation compound, respectively. We have found that the charge transfer from the intercalant layers to graphene layers is larger in KC_8 than in LiC_6 , opposite of what might be expected from their chemical composition. We have also measured the strength of the electron-phonon interaction on the graphene-derived Fermi surface to carbon derived phonons in both materials and found that it follows a universal trend where the coupling strength and superconductivity monotonically increase with the filling of graphene π^* states. This correlation suggests that both graphene-derived electrons and graphene-derived phonons are crucial for superconductivity in graphite intercalation compounds.

PACS numbers: 74.25.Kc, 71.18.+y, 74.10.+v

In graphite intercalation compounds (GIC), the intercalation of various atomic or molecular species in between graphene layers in graphite leads to novel properties and a very rich physics, including superconductivity [1]. In graphite intercalated with alkaline metals, superconductivity has been known for decades [2], but after recent discovery of relatively high T_c superconductivity in CaC_6 ($T_c = 11.5$ K) [3, 4] research in this field has been intensified. Even though the electron-phonon coupling (EPC) is most likely responsible for pairing in GICs [5–7], it is still not clear what electronic states, intercalant- or graphene-derived ones, and what phonons are responsible for pairing [8–11]. Due to differences in structure and composition, no clear trends have been identified that could unambiguously resolve these issues. For example, KC_8 is a superconductor and LiC_6 is not. Further, in GICs intercalated with alkaline earths, T_c ranges from zero to 11.5K, even though they share the same chemical formula MC_6 , where M is an alkaline earth atom. On the other hand, band structure calculations show that in graphite and GICs, an interlayer state exists above π^* band [12, 13], prompting some researchers to propose that its partial filling and coupling to soft intercalant phonons induces superconductivity in GICs [8, 14]. The experimental situation is still inconclusive, with strong advocates for intercalant [7] and graphene dominated superconductivity [5, 15–17]. Recent angle resolved photoemission spectroscopy (ARPES) study on CaC_6 [15] reported that EPC on graphene-derived Fermi surface (FS) to graphene phonons is strong enough to explain a T_c in the range of tens of Kelvin, indicating that graphene sheets provide crucial ingredients for superconductivity in GICs. However, to test this idea, it would be important to extend similar studies to GICs with different T_c .

In this letter, we report ARPES studies of the electronic structure and the EPC in the non-superconducting LiC_6 and in superconducting KC_8 ($T_c = 0.39$ K) and compare these materials with several other GICs. We find that the EPC on the graphene π^* states to the graphene derived phonons increases with the filling of π^* states in a sequence from LiC_6 to KC_8 to CaC_6 , following the same trend as T_c . The positive correlation between these quantities implies that superconductivity originates in graphene sheets while the main role of intercalants is to provide the charge for the graphene states.

The experiments were carried out on a Scienta SES-100 electron spectrometer operating in the angle-resolved mode at the beamline 12.0.1 of the Advanced Light Source. The spectra were recorded at the photon energy of 50 eV, with the combined instrumental energy resolution of 20–25 meV and the momentum resolution of $\pm 0.008 \text{ \AA}^{-1}$ in geometry where the polarization of light was perpendicular to the probed momentum line. The LiC_6 and KC_8 samples were prepared by intercalating natural, single-crystal graphite flakes (Madagascar) using the vapour transport method as described in Ref. [1]. X-ray diffraction showed very high sample purity with no graphite or secondary stage phases. To avoid degradation, all samples were unsealed and glued to the sample holder with Ag-epoxy in an Ar filled glow box. Protected by the epoxy, they were then quickly transferred to the ARPES prep-chamber, and cleaved at low temperature (15–20 K) under ultra-high vacuum conditions (2×10^{-9} Pa). All data were collected at 15–20 K.

Fig. 1 shows the ARPES spectra near the K point in the graphene Brillouin zone (BZ) for LiC_6 and KC_8 . The upper panels (a) and (b) show the contours of photoemission intensity as a function of binding energy for a

momentum line going through the K point. The intensity from a narrow interval (± 10 meV) around the Fermi level, representing the FS, is shown in the lower panels (c) and (d). The dispersing states are the graphene-derived π and π^* bands, as marked in Fig. 1(a) and (b). In KC_8 the low energy band structure is essentially graphene-like, with π and π^* bands touching at the Dirac point [16] which is shifted below the Fermi level due to doping. In LiC_6 , a sizable gap exists between π and π^* band. Dirac point is determined by extrapolating the linear part of π^* dispersion at low binding energies to the K point. The arrows in Fig. 1(a) and (b) indicate the position of Dirac point, (E_D), 0.825 eV and 1.35 eV for LiC_6 and KC_8 , respectively. It is clear from Fig. 1 that the π^* band is filled more in KC_8 than in LiC_6 and that it forms a larger FS (lower panels in Fig. 1) is a direct measure of doping of graphene π^* states, i.e. of the charge transferred into the graphene sheets. The FS is determined from peak positions of momentum distribution curves (MDCs) at E_F (open circles) and compared to the 3rd nearest neighbor hopping tight binding band structure (lines). In KC_8 , the occupied FS area is 0.399 \AA^{-2} which corresponds to 0.11 electrons per graphene unit cell (GUC), or 44% of the nominal value of 0.25 for the complete charge transfer. In LiC_6 , the occupied π^* (green circles and lines) FS area is 0.125 \AA^{-2} , corresponding to the doping of only 0.0344 electrons per GUC. This is far below the nominal value of 0.33 electrons per GUC.

The incomplete charge transfer into the graphene π^* states would suggest that the remaining charge occupies the so-called interlayer band. The occupation of the interlayer state has been recently reported in CaC_6 [18], but the observed feature was very weak and broad. Even the graphene-derived π^* state was very broad and did not form an enclosed contour at the Fermi level, casting doubts on these results. Our experiments always show relatively sharp π^* band that forms a well defined FS. However, in MC_6 (M=Li, Ca, Ba) materials, in addition to π^* band, we always see a broad feature at slightly higher binding energy that follows the π^* band, dispersing upward from K point (Fig. 1(a)). Further from the K point, the broad feature loses intensity and its dispersion cannot be precisely traced. In CaC_6 , this feature is observable over larger region of k space (Fig. 1 in [15]). It is possible be that this feature is a remnant of an interlayer band, smeared out by a disorder within the intercalant layers and folded into the K point of the graphene BZ. However, our measurements do not show any evidence of the interlayer band in the region from which it should be folded to the K point - the Γ point. We note that in pristine graphite, the interlayer hopping t_\perp splits both π and π^* bands into the bonding and antibonding counterparts due to the *AB* stacking of graphene sheets. It would be tempting to assign the broad feature as a bonding π^* state, due to similarities in initial dispersion. However,

all first stage GICs have the *AA* stacking of graphene sheets and such assignment would be incorrect. On the other hand, in LiC_6 and CaC_6 the π^* band might be split due to the *AB* stacking of the intercalant (if there is not too much disorder in the intercalant sites). If this was indeed the case, the correct charge transfer to the graphene layers would be 0.0616 and 0.349 electrons per GUC, for LiC_6 and for CaC_6 , respectively.

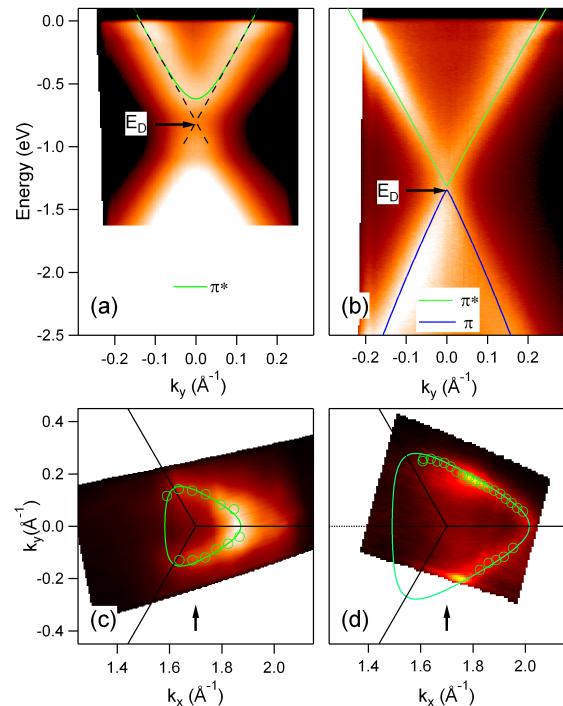


FIG. 1: Photoemission spectra from LiC_6 (a) and KC_8 (b) along the same momentum line in the graphene Brillouin Zone traversing the K point, as indicated by the arrows in panels (c) and (d). Lines represent the π and π^* bands. Arrows indicate the binding energy of Dirac point. (c) and (d) Photoemission intensity from a narrow energy interval around the Fermi level ($\omega = \pm 10$ meV), representing the graphene-derived π^* FS, for LiC_6 and KC_8 , respectively. Circles represent the MDC peak positions, while lines represent the tight-binding fits to the data, as described in the text.

Irrespective of these issues, our experimental observation that the doping of graphene sheets is larger in KC_8 than in LiC_6 is opposite of the expected nominal doping, but is in line with the existence of superconductivity in these materials: KC_8 is a superconductor and LiC_6 is not. In the following, we identify the reason for the correlation between superconductivity and doping of the graphene sheets. It is evident from Fig. 1 that in both LiC_6 and KC_8 , an anomaly or a kink in dispersion of the π^* band occurs at approximately 0.165 eV below the E_F . This is a hallmark of the interaction of the electronic states with phonons [19] that have been previously observed in CaC_6 and KC_8 [15, 16] and attributed to a coupling to

graphene in-plane high-frequency phonons. To quantify the electron phonon coupling, we have used the standard MDC fitting procedure [20, 21] which uses a tight binding dispersion as the starting approximation for the bare band and gives the real ($\text{Re}\Sigma$) and imaginary ($\text{Im}\Sigma$) part of self energy as fitting parameters. The bare band dispersion is then refined until the obtained $\text{Re}\Sigma$ and $\text{Im}\Sigma$ satisfy Kramers-Kronig transformations [22]. Panels (a) and (c) in Fig. 2 show the $\text{Im}\Sigma$ while panels (b) and (d) show $\text{Re}\Sigma$ for both materials for several different locations on the FS, as indicated in figure.

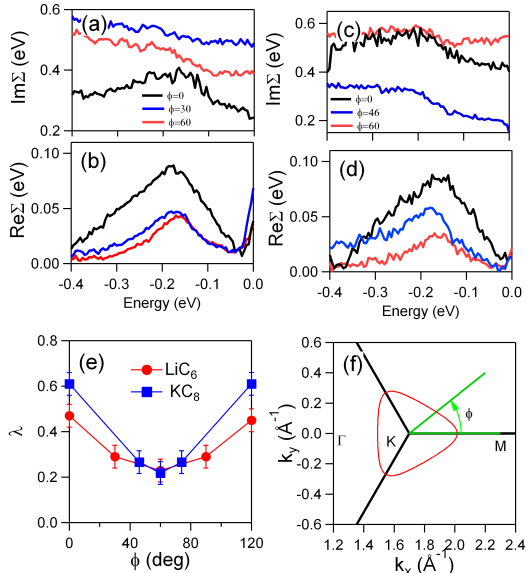


FIG. 2: $\text{Im}\Sigma(\omega)$ (a) and $\text{Re}\Sigma(\omega)$ (b) for LiC_6 and KC_8 ((c) and (d)) for several different points at the FS, as indicated in (e) and (f). (e) the electron-phonon coupling strength, λ , for LiC_6 and KC_8 , extracted from $\text{Re}\Sigma(\omega)$ as a function of polar angle ϕ as defined in (f).

$\text{Re}\Sigma$ in both materials shows a peak at around -0.165 eV, while $\text{Im}\Sigma$ shows a decrease below that energy, indicating a coupling to the phonon mode. The only phonons with such high energy are graphene-derived in-plane phonon modes. A small variation in the energy at which $\text{Re}\Sigma$ has a maximum at different points on the FS indicates a slight dispersion of the mode. We note that the sharp increase of $\text{Re}\Sigma$ below 20 meV is an artifact of finite energy resolution of the experimental apparatus [23]. We have excluded the affected interval $|\omega| < 20$ meV from the considerations and any fine structure, related to a possible coupling to the intercalant modes, is out of our detection limits. However, the lack of broadening of the π^* states with increasing temperature over the range of $15 \text{ K} < T < 200 \text{ K}$ suggests that the low energy modes play insignificant role and that the EPC is dominated by the graphene-derived high frequency modes.

The coupling constant λ can be extracted directly from

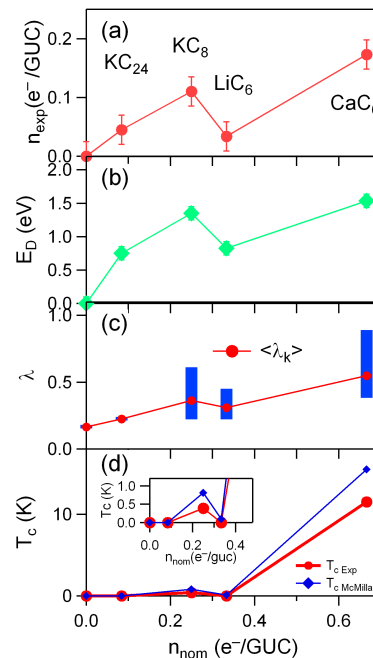


FIG. 3: (a) Measured charge transfer (electrons per graphene unit cell (GUC)) from the intercalant to the graphene π^* states. (b) Binding energy of Dirac point. (c) EPC coupling constant λ . The range of each vertical bar indicates the anisotropy with the maximum along the KM line and minimum along the K Γ line. Red circles represent the momentum-averaged coupling constant ($\langle\lambda_k\rangle$). (d) Superconducting transition temperature T_c in GICs. Red dots represent experimental values [2–4], and blue diamonds are calculated from the measured $\langle\lambda_k\rangle$, shown in (c), using McMillan's formula [24]. The inset zooms in the low T_c values. All the quantities are shown as functions of nominal chemical composition for measured GICs. Zero corresponds to the pristine graphite. Data for CaC_6 and pristine graphite are from ref. [15] and for KC_{24} are from ref. [25].

$\text{Re}\Sigma$ as ($\lambda = -[\partial(\text{Re}\Sigma)/\partial\omega]_0$) by fitting the low energy part to a straight line. It shows some anisotropy [Fig. 2(e)], with the maximum along the KM direction and the minimum along the K Γ direction, similar, but significantly smaller than in CaC_6 [15] and what was recently reported for KC_8 [16]. The most important observation, however, is that the momentum averaged $\langle\lambda_k\rangle$ is stronger in KC_8 than in LiC_6 . The coupling constant and its anisotropy both increase from LiC_6 to KC_8 to CaC_6 , exactly in the same sequence as the filling of the graphene π^* band and in previously established sequence for T_c . Strengthening of EPC with the filling of the π^* band has also been observed in the epitaxial graphene [26]. This is not surprising because the density of states near the E_F increases with the filling of the π^* band and a larger FS makes an EPC process more probable as the phase space available for the scattering events grows. In the pristine graphite, the FS is nearly a point and the

EPC is strongly suppressed [15, 27].

To better illustrate a positive correlation between T_c , λ and doping of the graphene π^* band in different GICs, we plot these quantities in Fig. 3 as functions of nominal chemical composition for several different materials. Actual (measured) charge transfer (in electrons/GUC) is shown in Fig. 3(a). The increase in size of the FS is consistent with the energy of Dirac point [panel (b)] as the chemical potential, μ , shifts from the pristine graphite to CaC_6 . It is interesting to note that $\mu \propto \sqrt{\bar{n}_{exp}}$ still holds, regardless of the shape of FS and number of FS sheets in these five different materials. The coupling constant λ and T_c follow the same trend. This suggests that the graphene π^* states and their coupling to graphene in-plane phonons is crucial for superconductivity and that the only role that the intercalants seem to play is to provide the charge for filling of the π^* states. This is further re-inforced by the calculated T_c using McMillan's formula [24]:

$$T_c = \frac{\Theta}{1.45} \exp\left(-\frac{1.04(\lambda + 1)}{\lambda - (0.62\lambda + 1)\mu^*}\right) \quad (1)$$

where we use measured $\langle \lambda_k \rangle$ (panel(c)), Debye temperature $\Theta = 1926$ K and Coulomb pseudo-potential $\mu^* \sim 0.14$. As shown in Fig. 3(d), the calculated T_c values are very close to the ones measured experimentally. The threshold-like behavior of T_c near $\langle \lambda_k \rangle = 0.3$ places LiC_6 on one side and KC_8 on another side of a steep increase in T_c . We note that superconductivity in LiC_3 and LiC_2 , materials in which more Li is pushed in under pressure, supports our picture where the EPC and superconductivity strengthen with the filling of graphene π^* states. The increase in T_c from 0.39 K for stoichiometric KC_8 to 0.55K in material with excess K is also in line with this picture. A further test would be a systematic ARPES study on alkaline-earth GICs (Ca, Sr, Ba) where T_c decreases with the atomic mass of alkaline-earth intercalant.

In conclusion, we have identified the universal trend in alkali and alkaline-earth GICs where superconductivity is tightly correlated with the doping of graphene-derived π^* states and with the coupling of these states to graphene phonons. This implies that the graphene sheets play the crucial role in superconductivity in GICs.

We acknowledge useful discussions with M. Calandra, M. Dean, M. Khodas, E. Rotenberg, M. Strongin and A. Walters. Work at Brookhaven is supported by the US DOE under Contract No. DE-AC02-98CH10886. Work at University College London is supported by the UK Engineering and Physical Science Research Council. ALS is operated by the US DOE under Contract No. DE-AC03-76SF00098.

- [1] M. Dresselhaus and G. Dresselhaus, *Adv. Phys.* **51**, 1 (2002).
- [2] N. B. Hannay, T. H. Geballe, B. T. Matthias, K. Andres, P. Schmidt, and D. MacNair, *Phys. Rev. Lett.* **14**, 225 (1965).
- [3] T. Weller, M. Ellerby, S. Saxena, R. Smith, and N. Skipper, *Nat. Phys.* **1**, 39 (2005).
- [4] N. Emery, C. Hérold, M. d'Astuto, V. Garcia, C. Bellin, J. F. Maréché, P. Lagrange, and G. Loupiau, *Phys. Rev. Lett.* **95**, 087003 (2005).
- [5] J. S. Kim, R. K. Kremer, L. Boeri, and F. S. Razavi, *Phys. Rev. Lett.* **96**, 217002 (2006).
- [6] G. Lamura, M. Aurino, G. Cifariello, E. Di Gennaro, A. Andreone, N. Emery, C. Hérold, J.-F. Maréché, and P. Lagrange, *Phys. Rev. Lett.* **96**, 107008 (2006).
- [7] D. G. Hinks, D. Rosenmann, H. Claus, M. S. Bailey, and J. D. Jorgensen, *Phys. Rev. B* **75**, 014509 (2007).
- [8] I. I. Mazin, *Phys. Rev. Lett.* **95**, 227001 (2005).
- [9] M. Calandra and F. Mauri, *Phys. Rev. Lett.* **95**, 237002 (2005).
- [10] L. Boeri, G. B. Bachelet, M. Giantomassi, and O. K. Andersen, *Phys. Rev. B* **76**, 064510 (2007).
- [11] I. I. Mazin, L. Boeri, O. V. Dolgov, A. A. Golubov, G. B. Bachelet, M. Giantomassi, and O. K. Andersen, *Physica C* **460**, 116 (2007).
- [12] M. Posternak, A. Baldereschi, A. J. Freeman, E. Wimmer, and M. Weinert, *Phys. Rev. Lett.* **50**, 761 (1983).
- [13] N. A. W. Holzwarth, S. G. Louie, and S. Rabii, *Phys. Rev. B* **30**, 2219 (1984).
- [14] G. Csanyi, P. Littlewood, A. Nevidomskyy, C. Pickard, and B. Simons, *Nat. Phys.* **1**, 42 (2005).
- [15] T. Valla, J. Camacho, Z.-H. Pan, A. V. Fedorov, A. C. Walters, C. A. Howard, and M. Ellerby, *Phys. Rev. Lett.* **102**, 107007 (2009).
- [16] A. Grüneis, C. Attaccalite, A. Rubio, D. V. Vyalikh, S. L. Molodtsov, J. Fink, R. Follath, W. Eberhardt, B. Büchner, and T. Pichler, *Phys. Rev. B* **79**, 205106 (2009).
- [17] M. P. M. Dean, C. A. Howard, S. S. Saxena, and M. Ellerby, *Phys. Rev. B* **81**, 045405 (2010).
- [18] K. Sugawara, T. Sato, and T. Takahashi, *Nat. Phys.* **5**, 40 (2009).
- [19] T. Valla, A. V. Fedorov, P. D. Johnson, and S. L. Hulbert, *Phys. Rev. Lett.* **83**, 2085 (1999).
- [20] S. LaShell, E. Jensen, and T. Balasubramanian, *Phys. Rev. B* **61**, 2371 (2000).
- [21] T. Valla, A. V. Fedorov, P. D. Johnson, J. Xue, K. E. Smith, and F. J. DiSalvo, *Phys. Rev. Lett.* **85**, 4759 (2000).
- [22] A. A. Kordyuk, S. V. Borisenko, A. Koitzsch, J. Fink, M. Knupfer, and H. Berger, *Phys. Rev. B* **71**, 214513 (2005).
- [23] T. Valla, *Phys. Rev. Lett.* **96**, 119701 (2006).
- [24] W. McMillan, *Phys. Rev.* **167**, 331 (1968).
- [25] J. Camacho, M. Upton, Z.-H. Pan, A. Walters, C. Howard, M. Ellerby, and T. Valla, unpublished.
- [26] J. L. McChesney, A. Bostwick, T. Ohta, K. V. Emtsev, T. Seyller, K. Horn, and E. Rotenberg, arXiv:0705.3264 (2007).
- [27] C. S. Leem, B. J. Kim, C. Kim, S. R. Park, T. Ohta, A. Bostwick, E. Rotenberg, H. D. Kim, M. K. Kim, H. J. Choi, et al., *Phys. Rev. Lett.* **100**, 016802 (2008).

* Electronic address: valla@bnl.gov